Observation and Reanalysis Derived Relationships Between Cloud and Land Surface Fluxes Across Cumulus and Stratiform Coupling Over the Southern Great Plains

Tianning Su[1,2], Zhanqing Li[1], Yunyan Zhang[2], Youtong Zheng[3,4], Haipeng Zhang[1]

[1]AOSC & ESSIC, University of Maryland at College Park, Maryland, 20740, USA
[2]Lawrence Livermore National Laboratory, Livermore, CA, USA
[3]Department of Earth and Atmospheric Science, University of Houston, Houston, TX, USA
[4]Institute for Climate and Atmospheric Science, University of Houston, Houston, TX, USA

*Corresponding authors: *zhanqing@umd.edu*; *su10@llnl.gov*

Key Points:

- This study develops a diagnostic approach for untangling cloud-land relationships across distinct cloud coupling regimes.
- Field observations are utilized to assess performances of reanalysis data in representing cloud-land interaction across different regimes.
- Findings emphasize the importance of differentiating cloud coupling regimes in observational and modeling studies of boundary layer clouds.

Keywords: clouds; land surface; sensible heat; reanalysis data; cloud-land coupling

Submission to ***Geophysical Research Letters***

Abstract. Understanding interactions between low clouds and land surface fluxes is critical to comprehending Earth's energy balance, yet their relationships remain elusive, with discrepancies between observations and modeling. Leveraging long-term field observations over the Southern Great Plains, this investigation revealed that cloud-land interactions are closely connected to cloud-land coupling regimes. Observational evidence supports a dual-mode interaction: coupled stratiform clouds predominate in low sensible heat scenarios, while coupled cumulus clouds dominate in high sensible heat scenarios. Reanalysis datasets, MERRA-2 and ERA-5, obscure this dichotomy owing to a shortfall in representing boundary layer clouds, especially in capturing the initiation of coupled cumulus in high sensible heat scenarios. ERA-5 demonstrates a relatively closer alignment with observational data, particularly in capturing relationships between cloud frequency and latent heat, markedly outperforming MERRA-2. Our study underscores the necessity of distinguishing different cloud coupling regimes, essential to the understanding of their interactions for advancing land-atmosphere interactions.

1 Introduction

Low clouds are key players in Earth's climate, influencing radiative balance and climate feedback loops. Continental low-level clouds are influenced by the land surface via processes occurring within the planetary boundary layer (PBL) (Betts, 2009; Teixeira and Hogan, 2002; Schumacher and Funk, 2023; Golaz et al., 2002; Berg and Kassianov, 2008; Yang et al., 2019; Guo et al., 2019; Zhang et al., 2017; Fast et al., 2019a). These clouds often emerge within the PBL's entrainment zone under convective conditions, yet their coupling with the land surface is complex and presents challenges in accurate determination and understanding (Su et al., 2022). Thus, a comprehensive examination of how terrestrial processes affect cloud evolution is warranted to understand the coupling of low-level clouds with the land surface (Bretherton et al., 2007; Moeng et al., 1996; Su et al., 2023; Xian et al., 2023; Zheng et al., 2021; Su and Li, 2024).

Extensive research has been carried out to investigate cloud-land interactions, highlighting the important roles of land surface heterogeneity, evaporative fraction, and soil moisture (Yue et al. 2017; Tang et al., 2019; Qian et al., 2023). Specifically, multiple studies have documented how land surface heterogeneity impacts the formation of shallow convection and development (Rieck et al. 2014; Xiao et al. 2018; Lee et al. 2019). Fast et al. (2019b) and Tao et al. (2019) have elucidated the strength of land-atmosphere interactions and their important roles in modulating convective cloud formation and evolution. As the majority of these studies have focused on local convection or cumulus, the wide range of cloud types and their interactions with the land surface present a complex and multifaceted challenge (Sakaguchi et al., 2022; Poll et al., 2022; Tao et al., 2021). It is essential to delve into these characteristics and dissect the cloud-land relationships across different regimes to achieve a more detailed understanding of these interactions.

Cloud variables in reanalysis data have also been extensively utilized in numerous studies (Su et al., 2013; Cesana et al., 2015), and have undergone detailed evaluations for the vertical structure and spatial variations (Dolinar et al., 2016; Free et al., 2016; Liu and Key, 2016). Several studies have reported the underestimation of low-level cloud fraction in popular reanalysis datasets, such as the European Centre for Medium-Range Weather Forecasts' fifth-generation global reanalysis (ERA-5), across different regions (Miao et al., 2019; Peng et al., 2019; Danso et al., 2019). Besides, reanalysis datasets face significant challenges in accurately representing the complex interactions between low clouds and the land surface (Tao et al., 2021; Wang et al., 2023; Betts et al., 2006). A gap exists in specifically assessing how these datasets capture cloud-land-surface coupling, particularly under stratiform regimes. Consequently, further investigation is warranted into the effectiveness of reanalysis products in representing the relationships between clouds and land surface fluxes across different coupling regimes.

Our study addresses two primary objectives: firstly, to develop a diagnostic approach for untangling cloud-land relationships across distinct cloud coupling regimes; and secondly, to evaluate the performance of prevailing reanalysis datasets in representing these relationships across different cloud regimes. Utilizing field observations over the Atmospheric Radiation Measurement (ARM) Southern Great Plains (SGP) site, we investigate the interactions between low clouds and land surface fluxes and highlight the discrepancies with reanalysis datasets for different cloud regimes, including coupled stratiform, coupled cumulus, and decoupled clouds.

2 Data and Method

2.1 Observational and reanalysis dataset

The ARM program, funded by the U.S. Department of Energy, has been operational at the SGP site in Oklahoma (36.607°N, 97.488°W) for decades. We use long-term data (1998-2020) over the SGP, including the Active Remote Sensing of Clouds (ARSCL, Clothiaux et al. 2000, 2001; Kollias et al. 2020), thermodynamic profiles from radiosonde, in-situ surface flux measurements, and meteorological data recorded at the surface (Cook, 2018; Xie et al., 2010). We further use reanalysis datasets from the ERA-5 (Hersbach et al., 2020) and Modern-Era Retrospective analysis for Research and Applications Version 2 (MERRA-2, Gelaro et al., 2017). As the state-of-art reanalysis data, the ERA-5 is produced by the Integrated Forecasting System (IFS) and a data assimilation system at a fine spatial resolution of 0.25° x 0.25°. Meanwhile, the MERRA-2 offers atmospheric and land information at a resolution of 0.5° x 0.625° (Randles et al., 2017). An important difference between the ERA-5 and MERRA-2 is the cloud parameterization: ERA-5 uses a prognostic cloud scheme (Tiedtke 1993) that accounts for the impacts from previous time steps whereas MERRA-2 uses a diagnostic cloud scheme. The procurement, processing, and quality assurance steps for observational and reanalysis datasets are further detailed in Supporting Information Section 1.

2.2 Identification of cloud coupling regimes

Su et al. (2022) developed a micropulse lidar-based approach to discern the cloud-land coupling by accounting for the vertical coherence and temporal continuity of PBL height (PBLH). Clouds are defined as coupled when the turbulence originating from the surface is able to reach the cloud base, thereby influencing its evolution, resulting in a turbulence-facilitated linkage among surface fluxes, PBL, and the cloud. We differentiate between coupled and decoupled low-level clouds using PBLH, cloud base, and lifting condensation level (LCL). The method for calculating PBLH is detailed in Su et al. (2020) which has been used to develop a PBLH climatological dataset at the central facilities of SGP. LCL values are calculated using the method outlined in Romps (2017). Coupled clouds are identified by the alignment of cloud base height (CBH) with the lidar-detected PBL top and LCL within a defined range, while decoupled clouds, which form independently of surface-driven updrafts, are indicated by a lack of this alignment.

Following the determination of cloud-land coupling, we exclude precipitation events exceeding 0.1 mm h^{-1} to prevent distortion in lidar signals and surface flux measurements. The study focuses on data from 09:00 to 15:00 Local Time (LT) to avoid the late afternoon period when the PBL typically begins to decay. We exclude the coexistence of coupled and decoupled low clouds during this period and further implement a classification into cumulus and stratiform categories among coupled cloud days. For coupled cumulus, two conditions are implemented in line with practices from previous studies (Zhang and Klein 2010, 2013; Lareau et al., 2018): (1) cloud formations must emerge after sunrise without low clouds at 08:00 LT to make sure that clouds are driven by local convection; (2) there is absence of overcast clouds. Coupled stratiform clouds are characterized by prolonged overcast clouds, which last more than 3 hours. Overcast low-level clouds have a cloud fraction of more than 90% based on ASRSL data.

Figure S1 showcases these cloud regimes, with coupled cumulus manifesting as discrete cellular formations in satellite imagery, and coupled stratiform clouds displaying broad, extensive coverage starting from the previous night. Meanwhile, decoupled clouds are distinguished by their separation from surface-driven PBL activity. Applying this methodological framework has led to the identification of 631 days marked by coupled cumulus and 470 days with coupled stratiform clouds across all seasons. In addition, we have distinguished 578 days with decoupled clouds across two decades, excluding instances with mixed coupled and decoupled low clouds.

Compared to the conventional approaches focused on identifying the specific types of clouds (e.g., cumulus or stratocumulus), our approach delineates different cloud-land coupling regimes, encompassing both coupled/decoupled states and cumulus/stratiform regimes. This enables a comprehensive analysis of cloud-land interactions, examining these relationships through the perspective of cloud-land coupling.

3 Results

3.1 Overall relationship between cloud occurrence frequency and surface fluxes

Our investigation begins by exploring the connection between the frequency of low cloud occurrences and surface sensible and latent heat fluxes. The evaluation criterion for low cloud occurrence is based on hourly cloud fraction where the maximum value between the surface and 700 hPa exceeds a 1% threshold. This study analyzes hourly mean data, with hourly low cloud occurrence categorized as 0 or 1. The cloud frequency is further calculated by dividing the sum by the total number of hours analyzed. This analysis incorporates data from both observational sources and the reanalysis datasets of ERA-5 and MERRA-2, as detailed in Figure 1. For the overall relationship, the same precipitation filter of 0.1 mm h^{-1} has been applied to the observation, ERA-5, and MERRA-2. Observational findings depicted in Figures 1a-b showcase a dual-mode interaction: cloud frequencies initially diminish at lower sensible heat levels and subsequently augment with an increase in sensible heat.

When extending the analysis to reanalysis datasets, different responses of cloud to surface fluxes emerge (Figures 1c-f). The correlation between surface fluxes observed and those within reanalysis datasets is presented in Figure S2. While ERA-5 partially captures the essence of the observed cloud-land relationships, particularly for latent heat, it still exhibits discrepancies in cloud frequency concerning sensible heat. ERA-5 data reflects a trend of decreasing cloud frequency with rising sensible heat, compared to the dual-mode interaction in the observations.

MERRA-2's response, however, is notably different; it presents a systematic underestimation of cloud occurrences across all surface flux ranges. Figure S3 accentuates this point by showing that both reanalysis datasets, especially MERRA-2, consistently underrepresent the average low cloud fractions across the spectrum of sensible and latent heat fluxes compared to observational data.

3.2 Characteristics for different cloud regimes

To elucidate the complex relationship between cloud presence and terrestrial influences, Figure 2 presents the changes of cloud occurrence frequency relative to surface sensible heat for different cloud regimes. By excluding days where low cloud regimes intermingle, we isolate the distinct behavioral signatures of each regime among days with coupled/decoupled scenarios and clear-sky. In the juxtaposition of reanalysis datasets against field observations, we examine the variation in cloud frequency under different levels of sensible heat in Figure 2. For comparison, these regimes of days are classified solely based on observational data and the relationships are calculated from observation and reanalysis data for the same samples.

Coupled stratiform clouds are characterized by their extensive coverage and cloud shading effects, predominating under low sensible heat conditions. As a result, there is a notable decrease in sensible heat concurrent with the increase in cloud frequency, as illustrated in Figures 2a-c. These clouds are associated with a well-mixed and unstable sub-cloud layer, indicative of a dynamic exchange of heat and moisture with the underlying surface, as depicted in Figure S4. The presence of widespread overcasting, often concurrent with lower sensible heat, reinforces the persistence of stratiform clouds by mitigating the drying effects of entrainment.

In the realm of coupled cumulus, an increase in sensible heat is linked to enhanced cloud formation, as surface heating intensifies convective activity within the PBL. During days when these clouds are present, ERA-5 data tend to underestimate the frequency of locally generated convection under high sensible heat scenarios, as reflected in Figure 2d-e. MERRA-2 demonstrates a significant deviation from observed patterns, consistently missing a large fraction of low clouds (Figure 2f). Decoupled clouds exhibit a more complex relationship with surface sensible heat (Figure 2g-i). Although they do not interact directly with PBL thermodynamics, they exert a cloud shading effect, leading to a suppression of surface sensible heat.

Figure 3 shows the relationships between cloud and latent heat. In analogy with the trends observed for sensible heat, coupled stratiform clouds demonstrate a diminishing frequency with increasing latent heat. On the other hand, coupled cumulus clouds tend to occur more frequently as latent heat increases, indicative of a conducive environment for cloud coupling, possibly through mechanisms such as lowering the LCL alongside PBL growth. This highlights that moderate to strong latent heat particularly promotes cloud formation coupling. To address the gap between grid and point data, we employed surface fluxes gridded to a spatial resolution of 0.25° x 0.25° for analyzing the cloud-land relationships, revealing that the patterns of these relationships exhibit similarity across both the gridded and point flux measurements (Figures S5 and Figure S6). In addition, stratiform cloud frequency generally increases with the evaporative fraction, emphasizing latent heat's role in their formation, while both ERA-5 and MERRA-2 inaccurately depict a decline in cloud frequency across evaporative fraction ranges and also fail to accurately represent cumulus formation at lower evaporative fraction values, which are primarily driven by sensible heat (Figure S7).

The diurnal variation in cloud fraction across the different regimes is further illustrated in Figure 4, which underscores the notable biases present in reanalysis datasets. MERRA-2 notably underestimates low-level cloud fractions. Despite a similar pattern, ERA-5 struggles to represent local cumulus convection and decoupled cloud scenarios with insufficient cloud fraction. Such underrepresentation of boundary layer clouds culminates in a generalized underestimation of low clouds within both MERRA-2 and ERA-5 (Figure S8). The underestimation in the low cloud fraction can also lead to a weak surface cooling effect in reanalysis data.

Our results are related to prior studies that highlight diurnal biases in convection over the central United States, particularly the challenges in accurately capturing local convection and the insufficient triggering of cumulus, as detailed in studies by Tao et al. (2021, 2023). Their studies also noted the shortfall in triggering shallow cumulus clouds, contributing to the biases in convection patterns.

3.3 Meteorological triggers for cloud formation across regimes

Cloud development across various coupling regimes is linked to essential meteorological factors, particularly atmospheric instability and humidity, as indicated by PBLH and surface relative humidity (RH_{sfc}). Figure 5a presents the coupling-decoupling difference, calculated as the difference between the frequencies of coupled and decoupled clouds, and examines its correlations with changes in PBLH and RH_{sfc}. Their relationships are also influenced by sensible heat marked in the grey-scale dots showing the connections between PBLH and RH_{sfc} under an array of sensible heat conditions. Figure 5b indicates the corresponding variations in the frequency of low clouds under different values of PBLH and RH_{sfc}.

Distinct domains emerge within the coupled cloud zone: more coupled stratiform clouds are prevalent in environments under higher RH_{sfc} and lower PBLH, typically associated with lower sensible heat conditions. Conversely, coupled cumulus clouds flourish under opposite conditions (i.e., lower RH_{sfc} and higher PBLH) suggestive of higher sensible heat and strong convection. Decoupled clouds, inferred from their negative coupling-decoupling differences, tend to occur towards lower PBLH across a broader RH spectrum, indicating their formation is less contingent on surface-induced convective processes. From low to high sensible heat, cloud regimes transit from coupled stratiform to coupled cumulus clouds.

Figures 5c-d present comparative analyses of the frequency of clouds vis-à-vis PBLH and RH_{sfc}, extracted from reanalysis datasets. Notably, both the occurrence and fraction of clouds are misrepresented in MERRA-2. While the ERA-5 clouds generally bear closer resemblance to the observed clouds, but still differ considerably in the occurrences of both coupled stratiform clouds and coupled cumulus. The underrepresentation of cumulus by the reanalysis stems from inadequate PBL development under high sensible heat scenarios (Figure 5c-d). Meanwhile, the RH is notably lower for the low sensible heat scenarios, which are linked with stratiform clouds. The systematic underestimation in RH can contribute to the overall underestimation of both cumulus and stratiform clouds, as illustrated in Figure S9, further hindering the triggering of coupled clouds. These findings underscore the critical need for enhancing the accuracy of surface flux and humidity representation in reanalysis datasets, alongside refining the parametrization of their effects on convection.

4. Discussion and Conclusions

In this study, we dissect the complex relationships between low clouds and surface fluxes over the Southern Great Plains. Building on previous studies that were primarily focused on cloud-land interactions within shallow cumulus, we demonstrate that both the cumulus and stratiform regimes represent distinct yet interconnected modes of cloud-land coupling. Consequently, we explore a bifurcated interaction pattern within the framework of cloud-land coupling, identifying that stratiform coupling prevails in low sensible heat conditions, while cumulus coupling becomes the leading regime in high sensible heat scenarios. Together, these findings portray the full paradigm of the coupling between cloud and land surface, occurring under various conditions. It follows from analyses of observations that meteorological conditions such as PBLH and RH are instrumental in cloud formation across different regimes, with transitions from stratiform to cumulus regimes leading to the overall pattern of cloud-land relationships.

Reanalysis datasets do not sufficiently capture the observed bifurcated interaction pattern and present a damped decline pattern in the cloud-land relationship. MERRA-2 consistently underestimates cloud frequency across various cloud regimes, with a particular shortfall in capturing the occurrence of coupled cumulus. ERA-5 generally exhibits a superior correlation with observational data, notably in the context of latent heat interactions. However, ERA-5 still shows discrepancies, especially with the frequency and initiation of coupled cumulus. Meanwhile, both reanalysis datasets fail to represent decoupled clouds accurately, as these clouds' formation mechanisms appear disconnected from local PBL processes.

This assessment of different cloud regimes underscores the significance of cloud coupling in analyzing cloud-land interactions. The initiation of convection in coupled cumulus is closely tied to surface processes on a sub-grid scale (Tian et al, 2022). As these cloud regimes respond to climate change, misrepresentation of these cloud dynamics within climate models could lead to uncertainties in predictions of climate sensitivity, as posited by Schneider et al. (2019). The emergence of global storm-resolving models with kilometer-scale resolutions, as detailed in Satoh et al. (2005), Caldwell et al. (2021) and Hohenegger et al. (2023), may offer great potential for addressing these complex modeling challenges in cloud-land interactions.

Acknowledgements: This work is supported by grants from the U.S. DOE (DE-SC0022919), the National Science Foundation (AGS2126098), and NASA (80NSSC21K1980). Y. Zheng is supported by the DOE Early Career Grant (DE-SC0024185). Y. Zhang is supported by the DOE Atmospheric System Research Science Focus Area THREAD project. Work at LLNL is performed under the auspices of the U.S. DOE by Lawrence Livermore National Laboratory under Contract DE-AC52-07NA27344.

Data Availability Statement: ARM radiosonde data, surface fluxes, and cloud masks are available online (ARM user facility. 1994). The identification for different cloud regimes for the study period is publicly available (Su, 2023). The data of planetary boundary layer are archived as an ARM product (Su and Li, 2023). Climate Data Store offers the ERA-5 reanalysis data (Hersbach et al. 2023). MERRA-2 reanalysis data can be downloaded online (GMAO, 2015).

References

Atmospheric Radiation Measurement (ARM) user facility. (1994). ARM Best Estimate Data Products (ARMBEATM). Southern Great Plains (SGP) Central Facility, Lamont, OK (C1). Compiled by C. Xiao and X. Shaocheng. [Dataset] ARM Data Center. http://dx.doi.org/10.5439/1333748.

Berg, L. K., and Kassianov, E.I. (2008): Temporal variability of fair-weather cumulus statistics at the ACRF SGP site. J. Climate, 21(13), 3344–3358.

Betts, A.K. (2009). Land ‐ surface ‐ atmosphere coupling in observations and models. Journal of Advances in Modeling Earth Systems, 1(3).

Betts, A.K., Ball, J.H., Barr, A.G., Black, T.A., McCaughey, J.H. and Viterbo, P., 2006. Assessing land-surface-atmosphere coupling in the ERA-40 reanalysis with boreal forest data. Agricultural and Forest Meteorology, 140(1-4), pp.365-382.

Bretherton, C. S., Blossey, P. N., and Uchida, J. (2007): Cloud droplet sedimentation, entrainment efficiency, and subtropical stratocumulus albedo. Geophys. Res. Lett., 34(3), L03813.

Caldwell, P.M., Terai, C.R., Hillman, B., Keen, N.D., Bogenschutz, P., Lin, W., Beydoun, H., Taylor, M., Bertagna, L., Bradley, A.M. and Clevenger, T.C., 2021. Convection‐permitting simulations with the E3SM global atmosphere model. Journal of Advances in Modeling Earth Systems, 13(11), p.e2021MS002544.

Cesana, G., Waliser, D.E., Jiang, X. and Li, J.L., 2015. Multimodel evaluation of cloud phase transition using satellite and reanalysis data. Journal of Geophysical Research: Atmospheres, 120(15), pp.7871-7892.

Clothiaux, E.E., Ackerman, T.P., Mace, G.G., Moran, K.P., Marchand, R.T., Miller, M.A. and Martner, B.E., 2000. Objective determination of cloud heights and radar reflectivities using a combination of active remote sensors at the ARM CART sites. Journal of Applied Meteorology and Climatology, 39(5), pp.645-665.

Clothiaux, E.E., Miller, M.A., Perez, R.C., Turner, D.D., Moran, K.P., Martner, B.E., Ackerman, T.P., Mace, G.G., Marchand, R.T., Widener, K.B. and Rodriguez, D.J., 2001. The ARM millimeter wave cloud radars (MMCRs) and the active remote sensing of clouds (ARSCL) value added product (VAP) (No. DOE/SC-ARM/VAP-002.1). DOE Office of Science Atmospheric Radiation Measurement (ARM) Program (United States).

Cook, D.R., 2018. Energy balance bowen ratio station (EBBR) instrument handbook (No. DOE/SC-ARM/TR-037). DOE Office of Science Atmospheric Radiation Measurement (ARM) Program (United States).

Danso, D.K., Anquetin, S., Diedhiou, A., Lavaysse, C., Kobea, A. and Touré, N.D.E., 2019. Spatio‐temporal variability of cloud cover types in West Africa with satellite‐based and reanalysis data. Quarterly Journal of the Royal Meteorological Society, 145(725), pp.3715-3731.

Dolinar, E.K., Dong, X. and Xi, B., 2016. Evaluation and intercomparison of clouds, precipitation, and radiation budgets in recent reanalyses using satellite-surface observations. Climate Dynamics, 46, pp.2123-2144.

Fast, J.D., Berg, L.K., Alexander, L., Bell, D., D’Ambro, E., Hubbe, J., Kuang, C., Liu, J., Long, C., Matthews, A. and Mei, F., 2019b. Overview of the HI-SCALE field campaign: A new perspective on shallow convective clouds. Bulletin of the American Meteorological Society, 100(5), pp.821-840.

Fast, J.D., Berg, L.K., Feng, Z., Mei, F., Newsom, R., Sakaguchi, K. and Xiao, H., 2019a. The impact of variable land‐atmosphere coupling on convective cloud populations observed during the 2016 HI‐SCALE field campaign. Journal of Advances in Modeling Earth Systems, 11(8), pp.2629-2654.

Free, M., Sun, B. and Yoo, H.L., 2016. Comparison between total cloud cover in four reanalysis products and cloud measured by visual observations at US weather stations. Journal of Climate, 29(6), pp.2015-2021.

Gelaro, R., McCarty, W., Suárez, M.J., Todling, R., Molod, A., Takacs, L., Randles, C.A., Darmenov, A., Bosilovich, M.G., Reichle, R. and Wargan, K., 2017. The modern-era retrospective analysis for research and applications, version 2 (MERRA-2). Journal of climate, 30(14), pp.5419-5454.

Global Modeling and Assimilation Office (GMAO) (2015), MERRA-2 tavg1_2d_rad_Nx: 2d,1-Hourly,Time-Averaged,Single-Level,Assimilation,Radiation Diagnostics V5.12.4, Greenbelt, MD, USA [Dataset]. Goddard Earth Sciences Data and Information Services Center (GES DISC), https://doi.org/10.5067/Q9QMY5PBNV1T.

Golaz, J.C., Larson, V.E. and Cotton, W.R. (2002). A PDF-based model for boundary layer clouds. Part I: Method and model description. Journal of the atmospheric sciences, 59(24), pp.3540-3551.

Guo, J., Su, T., Chen, D., Wang, J., Li, Z., Lv, Y., ... & Zhai, P. (2019). Declining summertime local - scale precipitation frequency over China and the United States, 1981 - 2012: The disparate roles of aerosols. Geophysical Research Letters, 46(22), 13281-13289.

Hersbach, H., Bell, B., Berrisford, P., Biavati, G., Horányi, A., Muñoz Sabater, J., Nicolas, J., Peubey, C., Radu, R., Rozum, I., Schepers, D., Simmons, A., Soci, C., Dee, D., Thépaut, J-N. (2023): ERA5 hourly data on pressure levels from 1940 to present. [Dataset] Copernicus Climate Change Service (C3S) Climate Data Store (CDS), DOI: 10.24381/cds.bd0915c6.

Hersbach, H., Bell, B., Berrisford, P., Hirahara, S., Horányi, A., Muñoz-Sabater, J., Nicolas, J., Peubey, C., Radu, R., Schepers, D. and Simmons, A., 2020. The ERA5 global reanalysis. Quarterly Journal of the Royal Meteorological Society, 146(730), pp.1999-2049.

Hohenegger, C., Korn, P., Linardakis, L., Redler, R., Schnur, R., Adamidis, P., Bao, J., Bastin, S., Behravesh, M., Bergemann, M. and Biercamp, J., 2023. ICON-Sapphire: simulating the components of the Earth system and their interactions at kilometer and subkilometer scales. Geoscientific Model Development, 16(2), pp.779-811.

Kollias, P., Bharadwaj, N., Clothiaux, E.E., Lamer, K., Oue, M., Hardin, J., Isom, B., Lindenmaier, I., Matthews, A., Luke, E.P. and Giangrande, S.E., 2020. The ARM radar network: At the leading edge of cloud and precipitation observations. Bulletin of the American Meteorological Society, 101(5), pp.E588-E607.

Lareau, N.P., Zhang, Y. and Klein, S.A. (2018). Observed boundary layer controls on shallow cumulus at the ARM Southern Great Plains site. Journal of the Atmospheric Sciences, 75(7), pp.2235-2255.

Lee, J.M., Zhang, Y. and Klein, S.A., 2019. The effect of land surface heterogeneity and background wind on shallow cumulus clouds and the transition to deeper convection. Journal of the Atmospheric Sciences, 76(2), pp.401-419.

Liu, Y. and Key, J.R., 2016. Assessment of Arctic cloud cover anomalies in atmospheric reanalysis products using satellite data. Journal of Climate, 29(17), pp.6065-6083.

Miao, H., Wang, X., Liu, Y. and Wu, G., 2019. An evaluation of cloud vertical structure in three reanalyses against CloudSat/cloud‐aerosol lidar and infrared pathfinder satellite observations. Atmospheric Science Letters, 20(7), p.e906.

Moeng, C.H., Cotton, W.R., Bretherton, C., Chlond, A., Khairoutdinov, M., Krueger, S., Lewellen, W.S., MacVean, M.K., Pasquier, J.R.M., Rand, H.A. and Siebesma, A.P. (1996). Simulation of a stratocumulus-topped planetary boundary layer: Intercomparison among different numerical codes. Bulletin of the American Meteorological Society, 77(2), pp.261-278.

Peng, X., She, J., Zhang, S., Tan, J. and Li, Y., 2019. Evaluation of multi-reanalysis solar radiation products using global surface observations. Atmosphere, 10(2), p.42.

Poll, S., Shrestha, P. and Simmer, C. (2022). Grid resolution dependency of land surface heterogeneity effects on boundary‐layer structure. Quarterly Journal of the Royal Meteorological Society, 148(742), pp.141-158.

Poll, S., Shrestha, P. and Simmer, C., 2022. Grid resolution dependency of land surface heterogeneity effects on boundary‐layer structure. Quarterly Journal of the Royal Meteorological Society, 148(742), pp.141-158.

Qian, Y., Guo, Z., Larson, V.E., Leung, L.R., Lin, W., Ma, P.L., Wan, H., Wang, H., Xiao, H., Xie, S. and Yang, B., 2023. Region and cloud regime dependence of parametric sensitivity in E3SM atmosphere model. Climate Dynamics, pp.1-17.

Randles, C.A., Da Silva, A.M., Buchard, V., Colarco, P.R., Darmenov, A., Govindaraju, R., Smirnov, A., Holben, B., Ferrare, R., Hair, J. and Shinozuka, Y., 2017. The MERRA-2 aerosol reanalysis, 1980 onward. Part I: System description and data assimilation evaluation. Journal of climate, 30(17), pp.6823-6850.

Rieck, M., Hohenegger, C. and van Heerwaarden, C.C., 2014. The influence of land surface heterogeneities on cloud size development. Monthly Weather Review, 142(10), pp.3830-3846.

Romps, D.M. (2017). Exact expression for the lifting condensation level. Journal of the Atmospheric Sciences, 74(12), pp.3891-3900.

Sakaguchi, K., Berg, L.K., Chen, J., Fast, J., Newsom, R., Tai, S.L., Yang, Z., Gustafson Jr, W.I., Gaudet, B.J., Huang, M. and Pekour, M., 2022. Determining spatial scales of soil moisture—Cloud coupling pathways using semi‐idealized simulations. Journal of Geophysical Research: Atmospheres, 127(2), p.e2021JD035282.

Satoh, M., Tomita, H., Miura, H., Iga, S., and Nasuno, T, 2005. Development of a global cloud resolving model – a multi-scale structure of tropical convections, J. Earth

Simulator, 3, 11–19.

Schneider, T., Kaul, C.M. and Pressel, K.G., 2019. Possible climate transitions from breakup of stratocumulus decks under greenhouse warming. Nature Geoscience, 12(3), pp.163-167.

Su, H., Jiang, J.H., Zhai, C., Perun, V.S., Shen, J.T., Del Genio, A., Nazarenko, L.S., Donner, L.J., Horowitz, L., Seman, C. and Morcrette, C. (2013). Diagnosis of regime‐dependent cloud simulation errors in CMIP5 models using "A‐Train" satellite observations and reanalysis data. Journal of Geophysical Research: Atmospheres, 118(7), pp.2762-2780.

Su, T, and Li, Z. (2023). Planetary Boundary Layer Height (PBLH) over SGP from 1998 to 2023. ORNL; ARM Archive; United States. [Dataset] https://doi.org/10.5439/2007149.

Su, T. (2023). Cloud Regime Identification over the SGP [Dataset]. Zenodo. https://doi.org/10.5281/zenodo.10437096.

Su, T., Li, Z. and Zheng, Y. (2023). Cloud‐Surface Coupling Alters the Morning Transition From Stable to Unstable Boundary Layer. Geophysical Research Letters, 50(5), p.e2022GL102256.

Su, T., Li, Z., and Kahn, R. (2020): A new method to retrieve the diurnal variability of planetary boundary layer height from lidar under different thermodynamic stability conditions. Remote Sens. Environ., 237, 111519.

Su, T., Zheng, Y., and Li, Z. (2022). Methodology to determine the coupling of continental clouds with surface and boundary layer height under cloudy conditions from lidar and meteorological data. Atmospheric Chemistry and Physics, 22(2), 1453-1466.

Su, T. and Li, Z., 2024. Decoding the Dialogue Between Clouds and Land. Eos, 105, https://doi.org/10.1029/2024EO240072.

Schumacher, C. and Funk, A., 2023. Assessing Convective-Stratiform Precipitation Regimes in the Tropics and Extratropics With the GPM Satellite Radar. *Geophysical Research Letters*, *50*(14), p.e2023GL102786.

Tang, S., Xie, S., Zhang, M., Tang, Q., Zhang, Y., Klein, S.A., Cook, D.R. and Sullivan, R.C., 2019. Differences in eddy-correlation and energy-balance surface turbulent heat flux measurements and their impacts on the large-scale forcing fields at the ARM SGP site. Journal of Geophysical Research: Atmospheres, 124(6), pp.3301-3318.

Tao, C., Xie, S., Ma, H.Y., Bechtold, P., Cui, Z., Vaillancourt, P.A., Choi, S.T., Wei, J., Wu, W.Y., Zhang, M. and Neelin13, J.D., 2023. Diurnal Cycle of Precipitation Over the Tropics and Central US: GCM Intercomparison. Quarterly Journal of the Royal Meteorological Society.

Tao, C., Zhang, Y., Tang, Q., Ma, H.Y., Ghate, V.P., Tang, S., Xie, S. and Santanello, J.A., 2021. Land–Atmosphere coupling at the US Southern Great Plains: A comparison on local convective regimes between ARM observations, reanalysis, and climate model simulations. Journal of Hydrometeorology, 22(2), pp.463-481.

Tao, C., Zhang, Y., Tang, S., Tang, Q., Ma, H.Y., Xie, S. and Zhang, M., 2019. Regional moisture budget and land‐atmosphere coupling over the US Southern Great Plains inferred from the ARM long‐term observations. Journal of Geophysical Research: Atmospheres, 124(17-18), pp.10091-10108.

Teixeira, J., and Hogan, T. F. (2002): Boundary layer clouds in a global atmospheric model: simple cloud cover parameterizations. J. Climate, 15(11), 1261–1276.

Tian, J., Zhang, Y., Klein, S.A., Öktem, R. and Wang, L., 2022. How does land cover and its heterogeneity length scales affect the formation of summertime shallow cumulus clouds in observations from the US Southern Great Plains?. Geophysical Research Letters, 49(7), p.e2021GL097070.

Tiedtke, M. (1993). Representation of clouds in large-scale models. Monthly Weather Review, 121(11), 3040-3061.

Wang, Y., Hu, J., Li, R., Song, B., Hailemariam, M., Fu, Y. and Duan, J., 2023. Increasing cloud coverage deteriorates evapotranspiration estimating accuracy from satellite, reanalysis and land surface models over East Asia. Geophysical Research Letters, 50(8), p.e2022GL102706.

Xian, T., Guo, J., Zhao, R., Su, T. and Li, Z., 2023. The impact of urbanization on mesoscale convective systems in the Yangtze River Delta region of China: insights gained from observations and modeling. Journal of Geophysical Research: Atmospheres, 128(3), p.e2022JD037709.

Xiao, H., Berg, L.K. and Huang, M. (2018). The impact of surface heterogeneities and land‐atmosphere interactions on shallow clouds over ARM SGP site. Journal of Advances in Modeling Earth Systems, 10(6), pp.1220-1244.

Xie, S., McCoy, R.B., Klein, S.A., Cederwall, R.T., Wiscombe, W.J., Clothiaux, E.E., Gaustad, K.L., Golaz, J.C., Hall, S.D., Jensen, M.P. and Johnson, K.L., 2010. Clouds and more: ARM climate modeling best estimate data: A new data product for climate studies. Bulletin of the American Meteorological Society, 91(LLNL-JRNL-412676).

Yang, Y.J., Wang, H., Chen, F., Zheng, X., Fu, Y. and Zhou, S., 2019. TRMM-based optical and microphysical features of precipitating clouds in summer over the Yangtze–Huaihe River valley, China. Pure and Applied Geophysics, 176, pp.357-370.

Yue, Q., Kahn, B.H., Fetzer, E.J., Wong, S., Frey, R. and Meyer, K.G., 2017. On the response of MODIS cloud coverage to global mean surface air temperature. Journal of Geophysical Research: Atmospheres, 122(2), pp.966-979.

Zhang, M., Wang, X., Chen, J., Cheng, T., Wang, T., Yang, X., Gong, Y., Geng, F. and Chen, C. (2010). Physical characterization of aerosol particles during the Chinese New Year's firework events. Atmospheric Environment, 44(39), pp.5191-5198.

Zhang, Y. and Klein, S.A. (2010). Mechanisms affecting the transition from shallow to deep convection over land: Inferences from observations of the diurnal cycle collected at the ARM Southern Great Plains site. Journal of the Atmospheric Sciences, 67(9), pp.2943-2959.

Zhang, Y. and Klein, S.A., 2013. Factors controlling the vertical extent of fair-weather shallow cumulus clouds over land: Investigation of diurnal-cycle observations collected at the ARM Southern Great Plains site. Journal of the Atmospheric Sciences, 70(4), pp.1297-1315.

Zhang, Y., Klein, S.A., Fan, J., Chandra, A.S., Kollias, P., Xie, S. and Tang, S., 2017. Large-eddy simulation of shallow cumulus over land: A composite case based on ARM long-term observations at its Southern Great Plains site. Journal of the Atmospheric Sciences, 74(10), pp.3229-3251.

Zheng, Y., Zhang, H., Rosenfeld, D., Lee, S.S., Su, T. and Li, Z. (2021). Idealized large-eddy simulations of stratocumulus advecting over cold water. Part I: Boundary layer decoupling. Journal of the Atmospheric Sciences, 78(12), pp.4089-4102.

Additional References in Supporting Information

Wesely, M. L., Cook, D. R., and Coulter, R. L. (1995): Surface heat flux data from energy balance Bowen ratio systems (No. ANL/ER/CP-84065; CONF-9503104-2). Argonne National Lab., IL (United States).

Schaaf, C.B., Gao, F., Strahler, A.H., Lucht, W., Li, X., Tsang, T., Strugnell, N.C., Zhang, X., Jin, Y., Muller, J.P. and Lewis, P., 2002. First operational BRDF, albedo nadir reflectance products from MODIS. Remote sensing of Environment, 83(1-2), pp.135-148.

Holdridge, D., Ritsche, M., Prell, J., and Coulter, R. (2011): Balloon-borne sounding system (SONDE) handbook, https://www.arm.gov/capabilities/instruments/sonde.

Figures

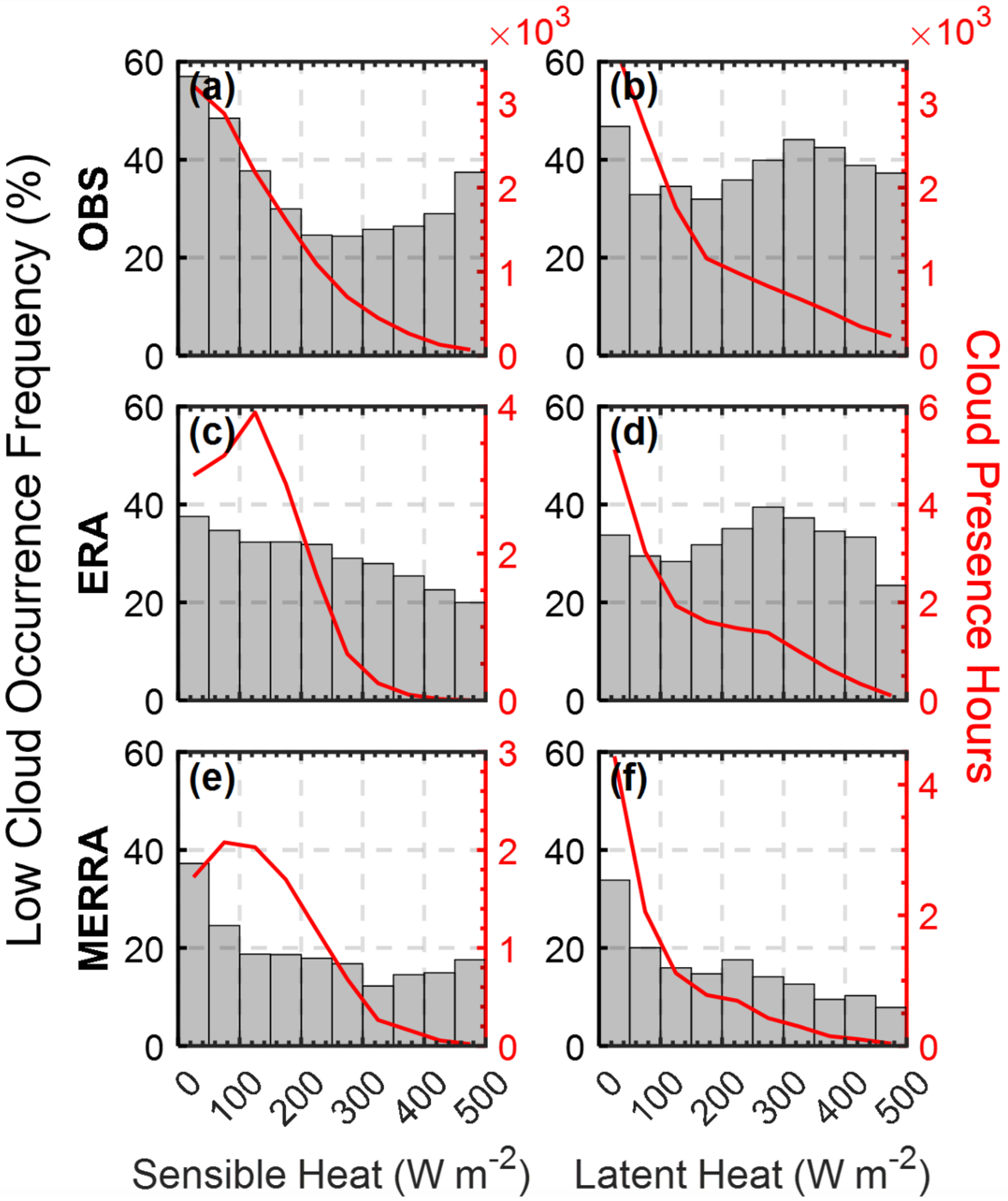

Figure 1. Comparison of observations and reanalysis for the relationships between low clouds and surface fluxes. Histograms represent the average frequency of low cloud occurrences binned by surface sensible heat (a, c, e) and latent heat flux (b, d, f) during 09:00-15:00 LT. Red lines indicate the number of hours with low cloud occurrence within each flux bin. Cases with precipitation exceeding 0.1mm h^{-1} are excluded from analyses. The first (a, b), second (c, d), and third rows (e, f) correspond to observations, ERA-5, and MERRA-2 respectively.

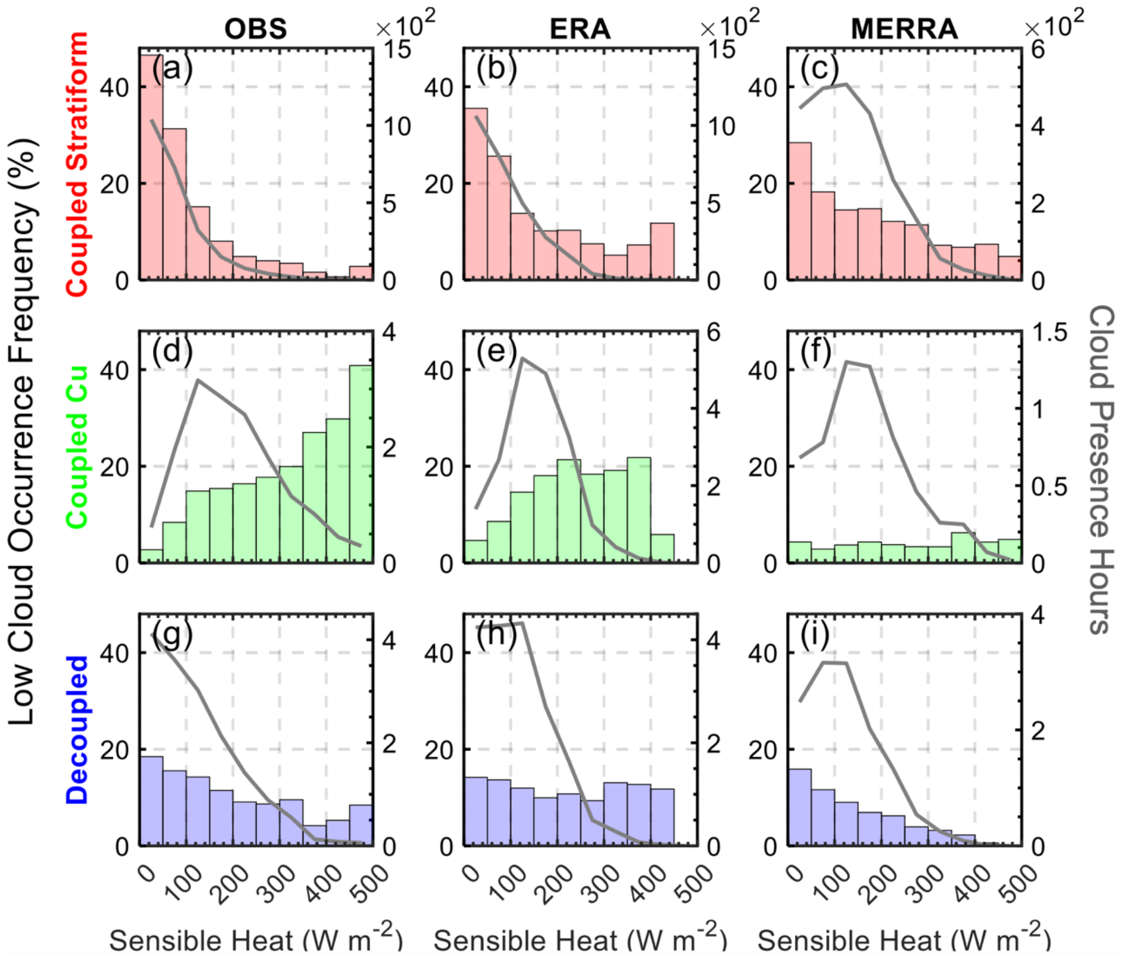

Figure 2. Cloud occurrence frequency and surface sensible heat relationships segregated by conditions of cloud regimes during 09:00-15:00 LT. The histograms display the average frequency of different cloud types binned by surface sensible heat flux for observational (OBS), ERA reanalysis, and MERRA reanalysis datasets. Panels (a) to (c) showcase coupled stratiform clouds, panels (d) to (f) depict coupled cumulus clouds, and panels (g) to (i) present decoupled clouds. Grey lines indicate the number of hours with low cloud occurrence within each flux bin.

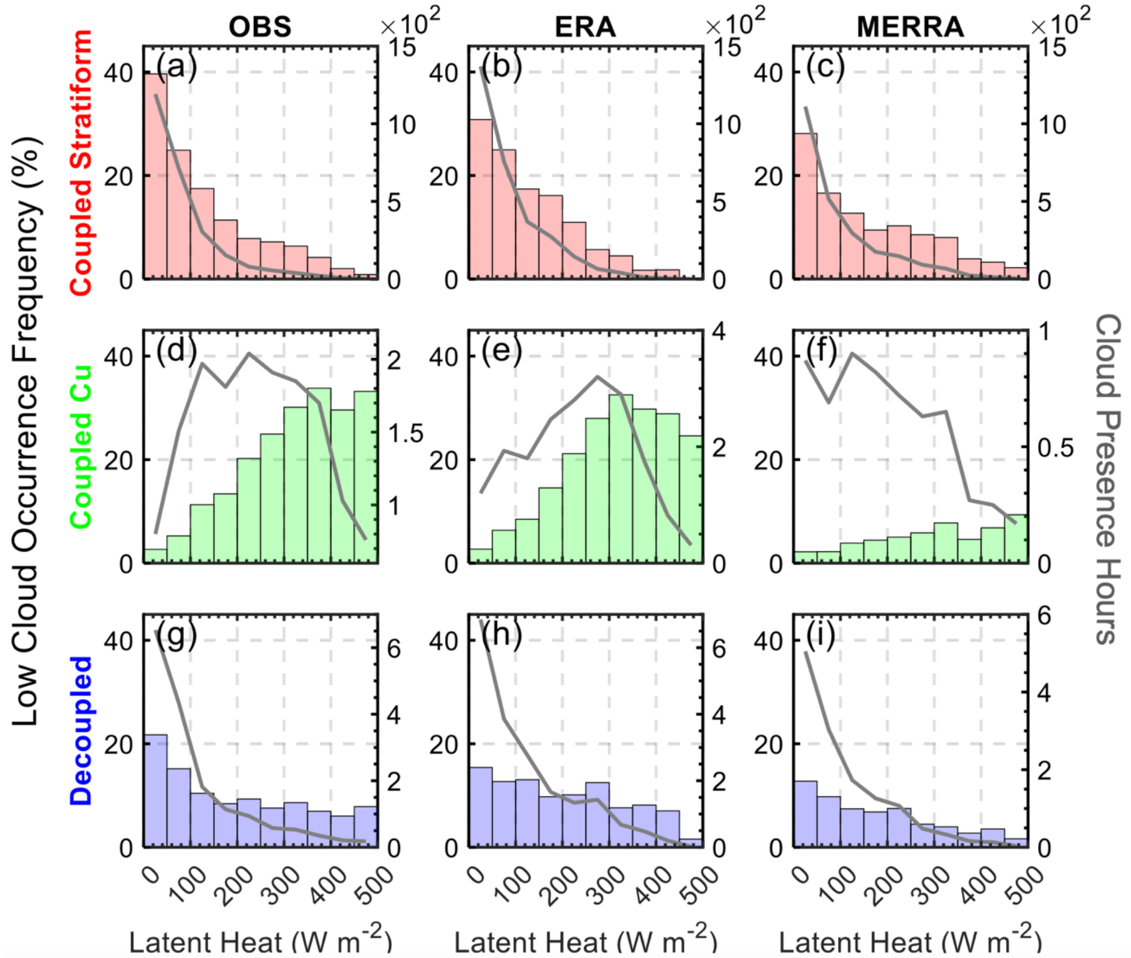

Figure 3. Similar to Figure 2, but depicting the relationships between low cloud occurrence frequency and surface latent heat fluxes.

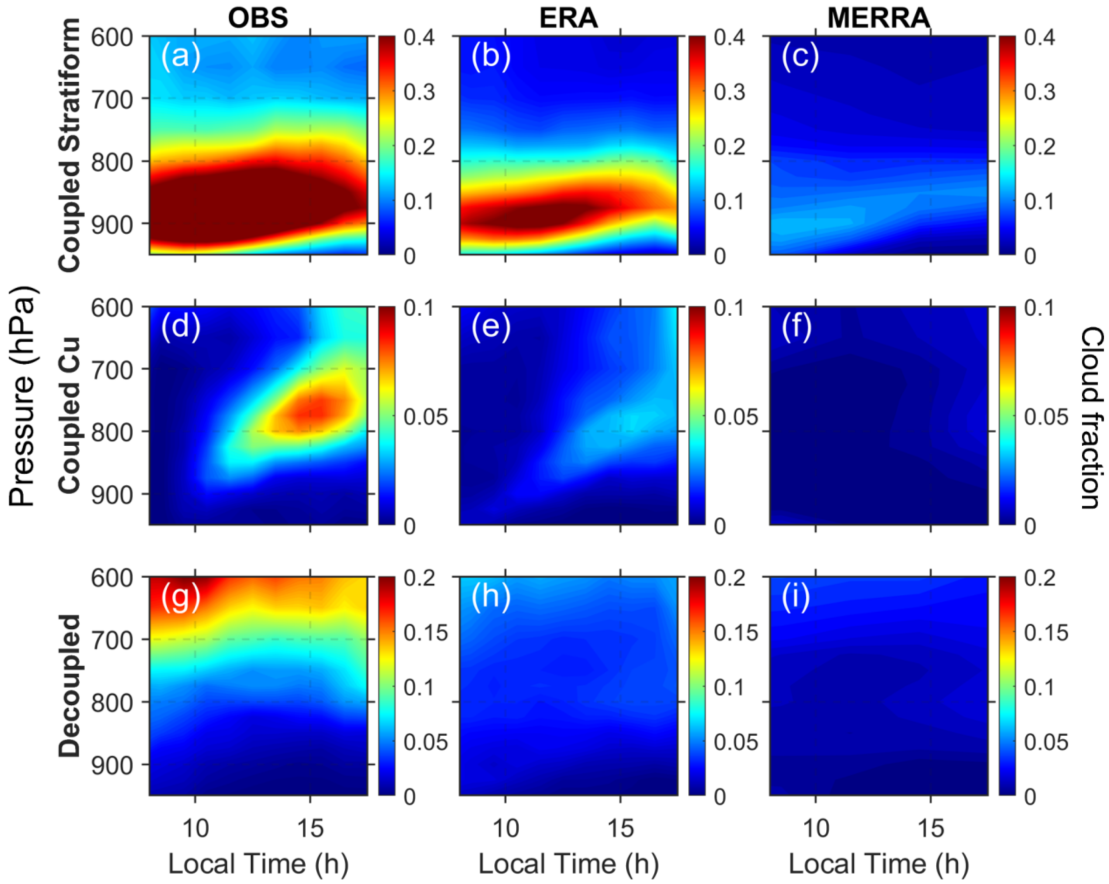

Figure 4. Diurnal variation of cloud fraction with atmospheric pressure across different cloud regimes in observations and reanalysis data. This figure presents contour plots that display the variation of cloud fraction during the daytime at various atmospheric pressures for three distinct scenarios: coupled stratiform clouds, coupled cumulus, and decoupled clouds. Each row represents one of the cloud scenarios, with observational data (OBS) in the first column, ERA reanalysis data in the second column, and MERRA reanalysis data in the third column.

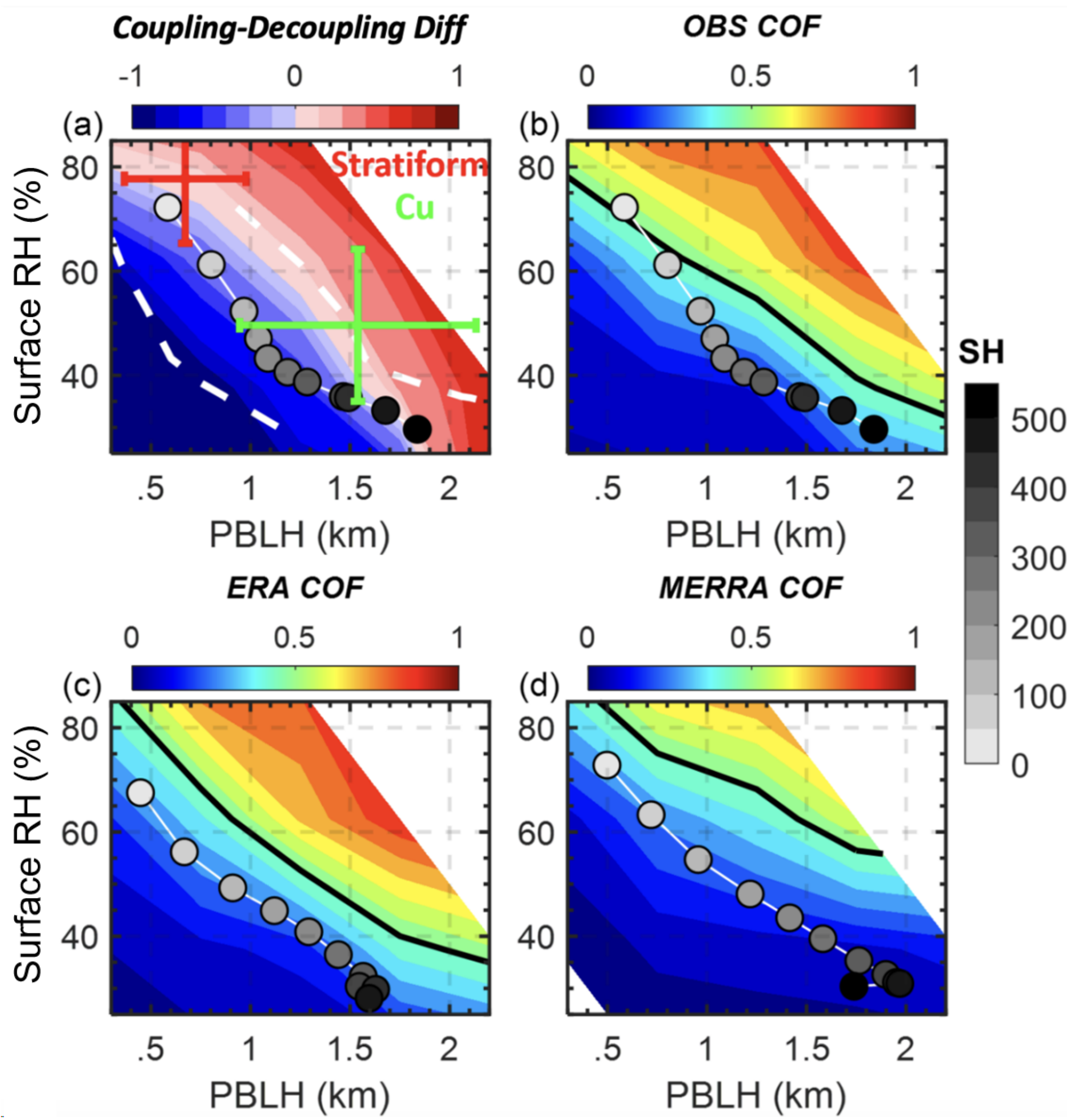

Figure 5. (a) The differences between the frequencies of coupled and decoupled clouds (former minus latter) under the different ranges of Planetary Boundary Layer Height (PBLH) and surface relative humidity (RH_{sfc}). (b-d) The values of the low cloud occurrence frequency (COF) correspond to PBLH and RH_{sfc} from (b) observations, (c) ERA-5, and (d) MERRA-2. In (a), the means and standard deviations of stratiform clouds and cumulus are marked. The grey-scale dots indicate the averages of PBLH and RH_{sfc} for different sensible heat values. The dash white lines in (a) indicate the range of standard deviations of different PBLH for different sensible heat bins. The black line denoting the position of 50% COF.

AGU PUBLICATIONS

Supporting Information for

Observation and Reanalysis Derived Relationships Between Cloud and Land Surface Fluxes Across Cumulus and Stratiform Coupling Over the Southern Great Plains

Tianning Su[1,2], Zhanqing Li[1], Yunyan Zhang[2], Youtong Zheng[3,4], Haipeng Zhang[1]

[1]AOSC & ESSIC, University of Maryland at College Park, Maryland, 20740, USA

[2]Lawrence Livermore National Laboratory, Livermore, CA, USA

[3]Department of Earth and Atmospheric Science, University of Houston, Houston, TX, USA

[4]Institute for Climate and Atmospheric Science, University of Houston, Houston, TX, USA

*Corresponding authors: zhanqing@umd.edu; su10@llnl.gov

Contents of this file

This PDF file includes:

Text S1
Figs. S1 to S9

S. 1 Descriptions of datasets:

(1) Thermodynamic profiles from radiosonde

We will use radiosonde measurements to characterize the thermodynamic settings of the PBL. Radiosondes are routinely launched multiple times at the ARM sites. Holdridge et al. (2011) provided technical details about the ARM radiosonde. Using the well-established method developed by Liu and Liang (2010), we retrieved PBLHs over the SGP site based on the vertical profiles of potential temperature from radiosonde measurements.

(2) Active Remote Sensing of Clouds (ARSCL)

We will use the well-established ARM cloud product, named ARSCL, generated for each ARM site (Clothiaux et al., 2000; Flynn et al., 2017). ARSCL provides the vertical boundaries of clouds by combining data from the MPL, ceilometer, and cloud radar, conveying useful information pertaining to the vertical structure and temporal evolution of clouds (Kollias et al., 2007). For the lowest cloud base, we will use the best estimation from laser-based techniques (i.e., MPL and ceilometer). Based on ARSCL, Xie et al. (2010) offers a comprehensive dataset of cloud fraction profiles.

(3) Surface fluxes

Surface fluxes are critical for PBL development and closely interact with low clouds as the driving force. A value-added product at ARM called the bulk aerodynamic latent and sensible heat fluxes from energy balance Bowen ratio (BAEBBR) was generated to replace energy balance Bowen ratio flux measurements with a bulk aerodynamic estimation when the Bowen Ratio (Wesely et al., 1995). We use the Best Estimate

Sensible/Latent Heat Fluxes in the BAEBBR product.

(4) ARMBE2DGRID

The ARMBE2DGRID VAP provides a dataset by integrating key surface measurements from the Southern Great Plains sites, consolidating them into a uniform 2D grid (https://www.arm.gov/capabilities/science-data-products/vaps/armbe2dgrid). The dataset delivers hourly data with a spatial resolution of 0.25° x 0.25°. It encompasses a wide range of products including Surface Meteorological Instrumentation, data from Oklahoma Mesonet and Kansas State University Mesonet, Quality Controlled Radiation Data, observations from Geostationary Operational Environmental Satellites, Microwave Radiometer, Best-Estimate Fluxes from BAEBBR, ECOR outputs, and Soil Water and Temperature System data. Rigorous Quality Controls are employed to ensure the reliability of the data.

(5) MODIS aboard the NASA Aqua and Terra

NASA's Aqua and Terra satellites, carrying the Moderate Resolution Imaging Spectroradiometer (MODIS), provides high-quality data on global cloud coverage. The corrected reflectance product from MODIS offers a true-color view of the Earth's surface and atmosphere, allowing for accurate confirmation of cloud presence and extent (Schaaf et al., 2002). By analyzing the true-color imagery, we can inspect cloud regimes, checking stratiform and cumulus for coupled clouds. NASA MODIS imageries are achieved in https://worldview.earthdata.nasa.gov/.

(6) ERA-5 Reanalysis Data

As one of the most advanced and widely used reanalysis data, ERA-5, produced by the European Centre for Medium-Range Weather Forecasts (ECMWF), provides a high-resolution, hourly updated global atmospheric reconstruction (Hersbach et al. 2020). Utilizing advanced assimilation of vast amounts of observational data, ERA-5 offers comprehensive climate variables, including temperature, humidity, wind, and cloud properties. We used this dataset to compare cloud-land relationships between observation and reanalysis datasets. With its fine spatial resolution and temporal coverage, ERA-5 allows for analysis of cloud formation, relating to PBL thermodynamics and surface processes.

(7) MERRA-2 Reanalysis Data

The Modern-Era Retrospective analysis for Research and Applications, Version 2 (MERRA-2), developed by NASA, is an improved reanalysis dataset focusing on the representation of the hydrological cycle, aerosols, and atmospheric composition (Gelaro et al., 2017). MERRA-2 integrates satellite and ground-based observational data to provide a coherent record of the global atmosphere. The low cloud fraction data are provided at a temporal resolution of one hour, while the vertical cloud fraction are available at three-hour intervals. In this study, MERRA-2's extensive coverage and detailed depiction of atmospheric variables are used to examine the cloud occurrences and their relationship with surface fluxes.

685 **Figures**

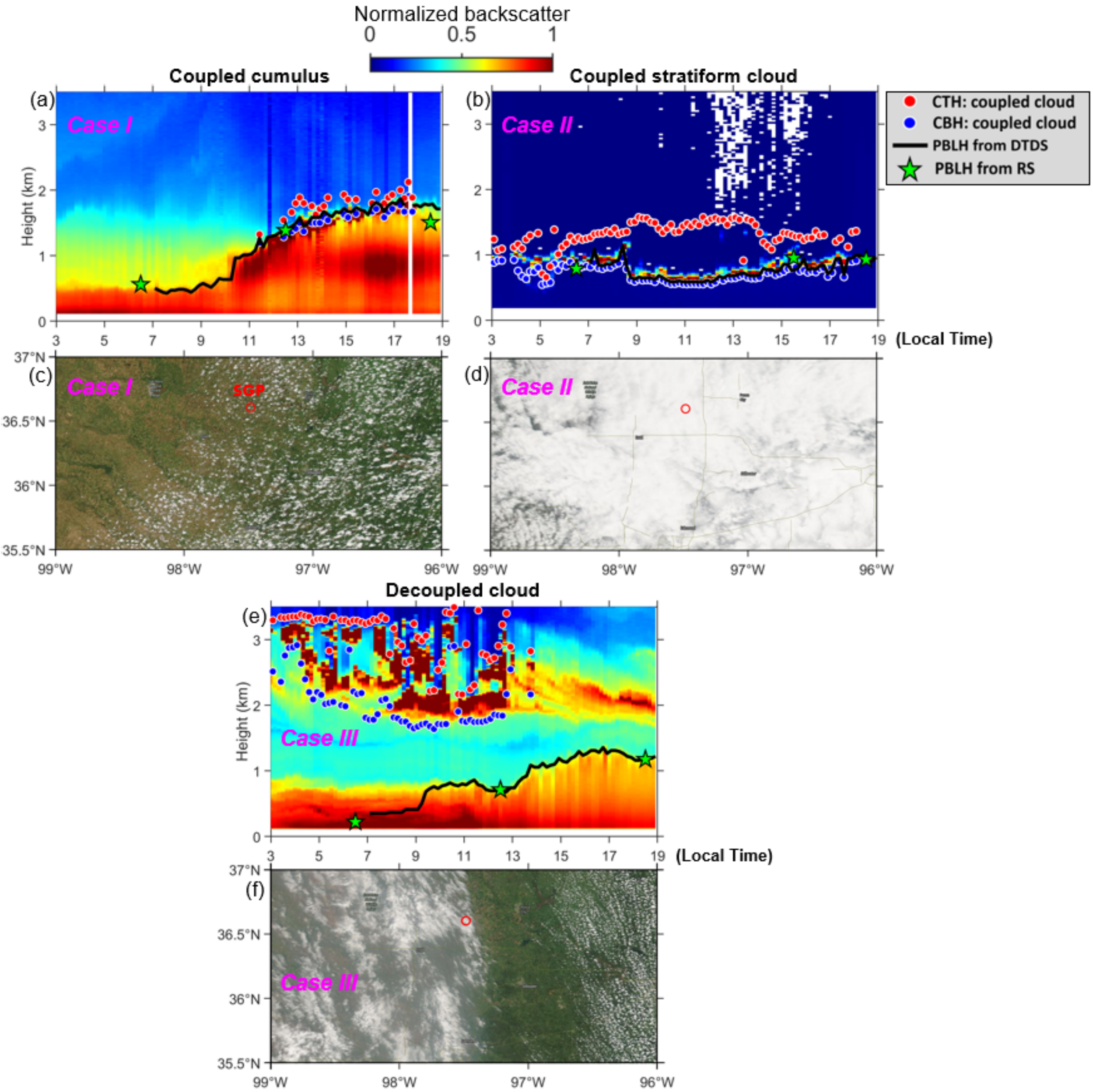

686

687 **Figure S1.** Daily vertical profiles of backscatters for coupled cumulus (a, Case I) and
688 coupled stratiform cloud (b, Case II). Backscatter is normalized to a range of 0-1, in
689 arbitrary units. Red dots and blue dots indicate the CTH and CBH of coupled cloud.
690 Black lines and green stars mark the PBLH retrieved from MPL and radiosonde. (c and
691 d) 2-D view of the corrected reflectance (true color) derived from MODIS (Aqua) for
692 Case I (c) and Case II (d). The red circle marks the position of SGP site. (e-f) Daily

vertical profiles of backscatters and the satellite image for decoupled cloud (Case III).

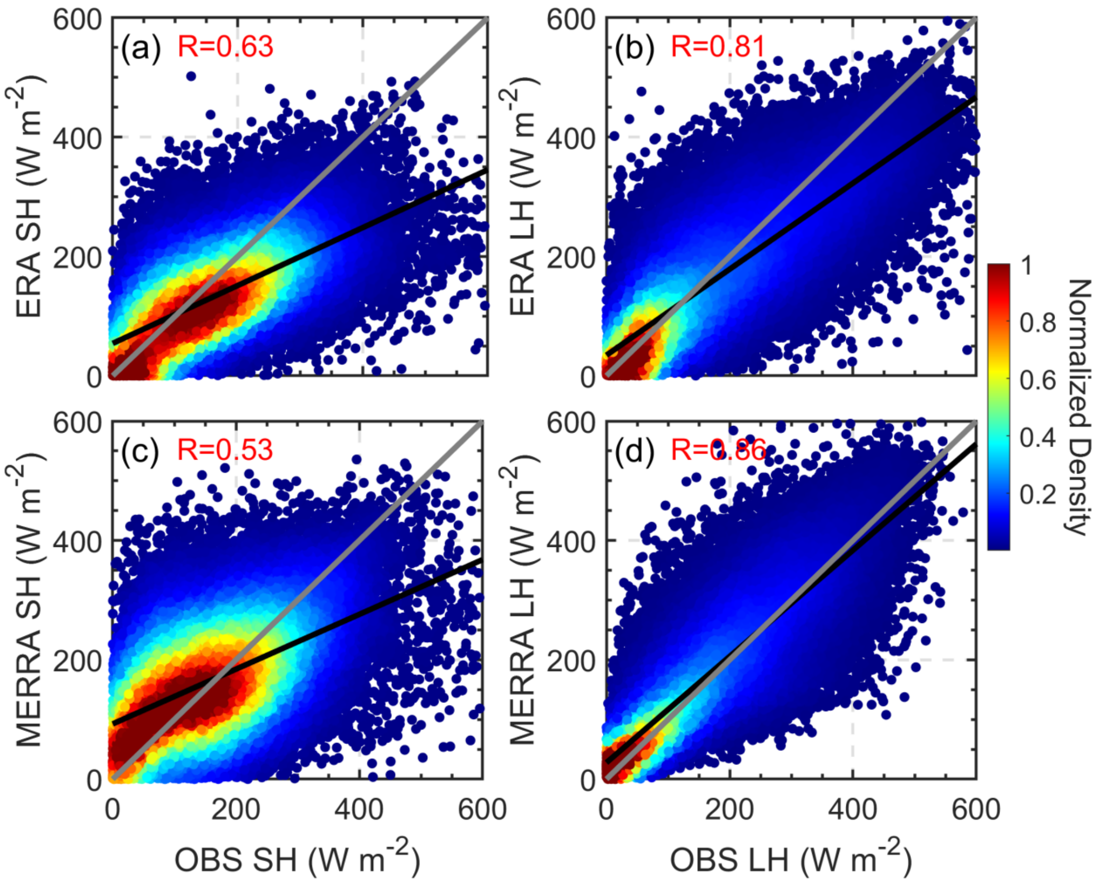

Figure S2. Density scatterplots of the comparison between observed surface fluxes and reanalysis surface fluxes during 09:00-15:00 Local Time (OBS SH: observed sensible heat; OB LH: observed latent heat; ERA SH: sensible heat from ERA-5; ERA LH: latent heat from ERA-5; MERRA SH: sensible heat from MERRA-2; MERRA LH: latent heat from MERRA-2). The correlation coefficients (R) are given in each panel. The solid black lines represent the linear regression, and the dashed grey lines denote 1:1 line.

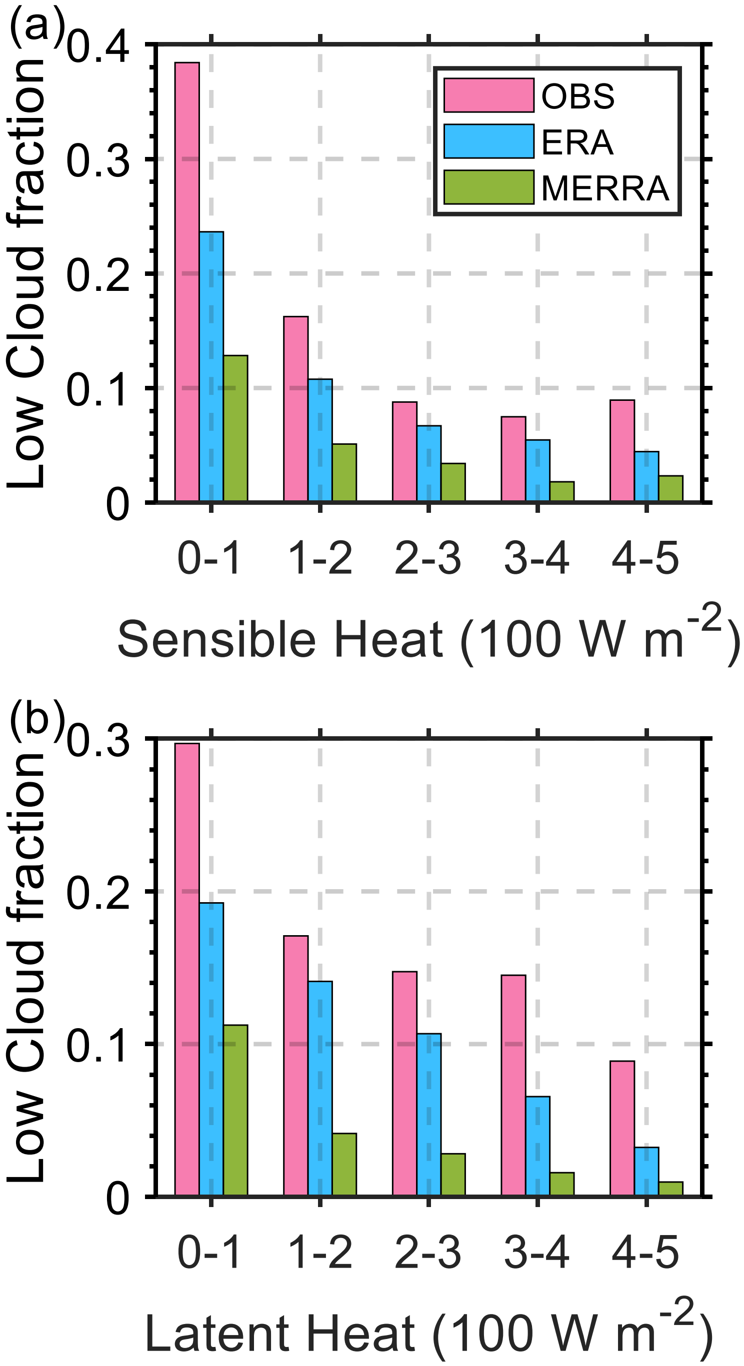

Figure S3. Comparison of average low cloud fraction across varying ranges of sensible and latent heat fluxes. The low cloud fraction is defined as the maximum cloud fraction occurring between the surface and 700 hPa. The data are categorized by source, with observations (OBS), ERA-5, and MERRA-2 depicted in pink, blue, and green bars, respectively.

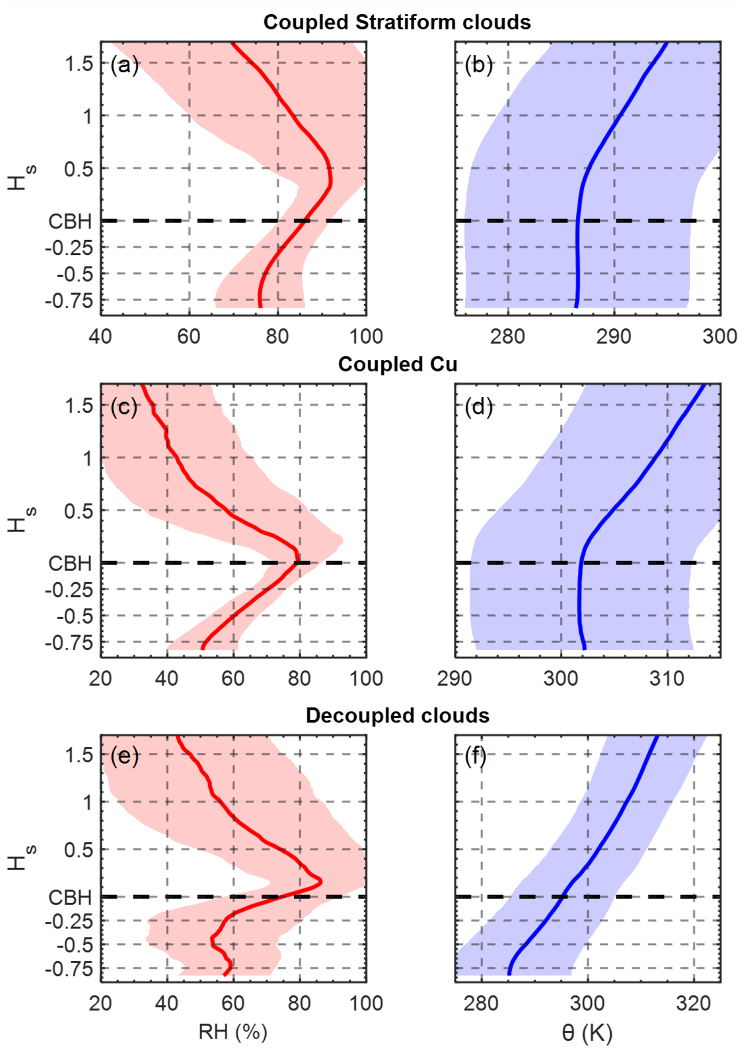

Figure S4. The average profiles of RH (red line) and virtual potential temperature (θ_v, blue line) for (a) coupled stratiform cloud, (b) coupled cumulus, and (c) decoupled cloud. The vertical scale is normalized by CBH (black dash line). The red and blue shaded areas indicate the standard deviations for RH and virtual potential temperature, respectively.

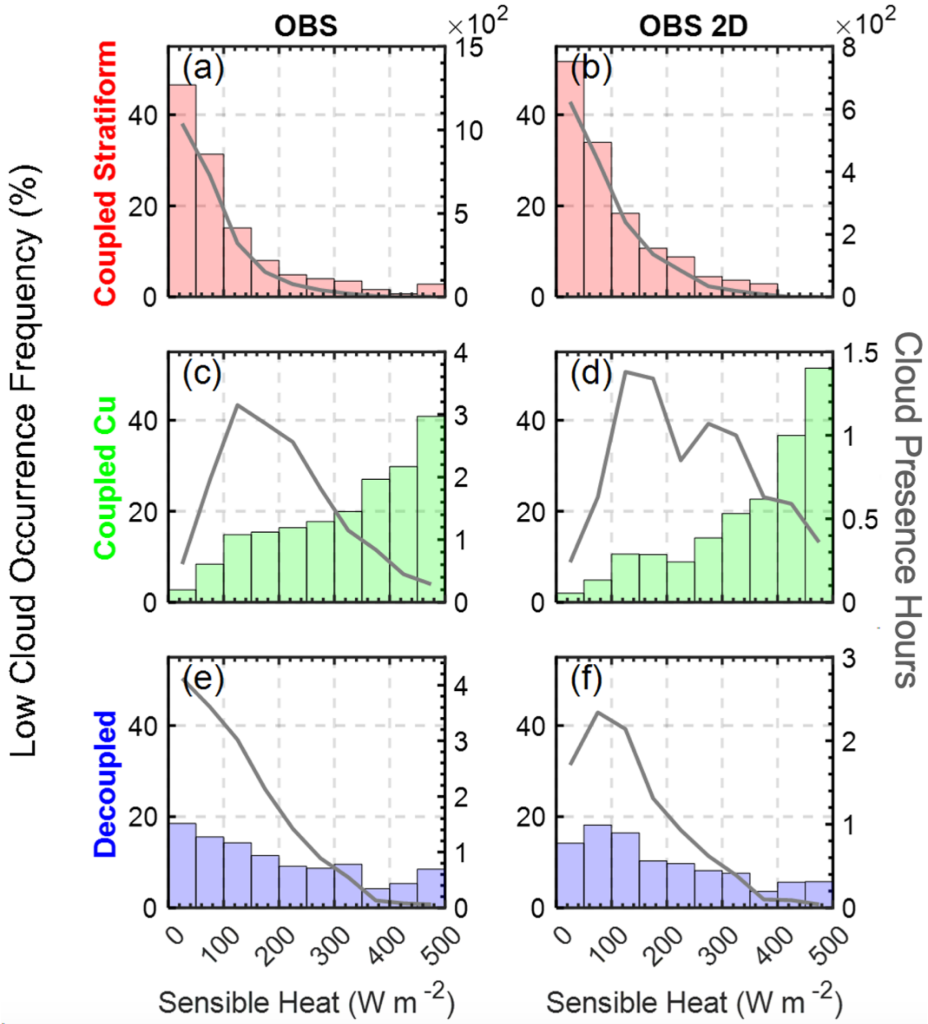

Figure S5. Cloud occurrence frequency and surface sensible heat relationships segregated by conditions of cloud regimes during 09:00-15:00 LT. The histograms display the average frequency of different cloud types binned by surface sensible heat flux for point observation (OBS) from the BAEBBR and for the 2D observation (OBS 2D) from the ARMBE2DGRID. Grey lines indicate the number of hours with low cloud occurrence within each flux bin.

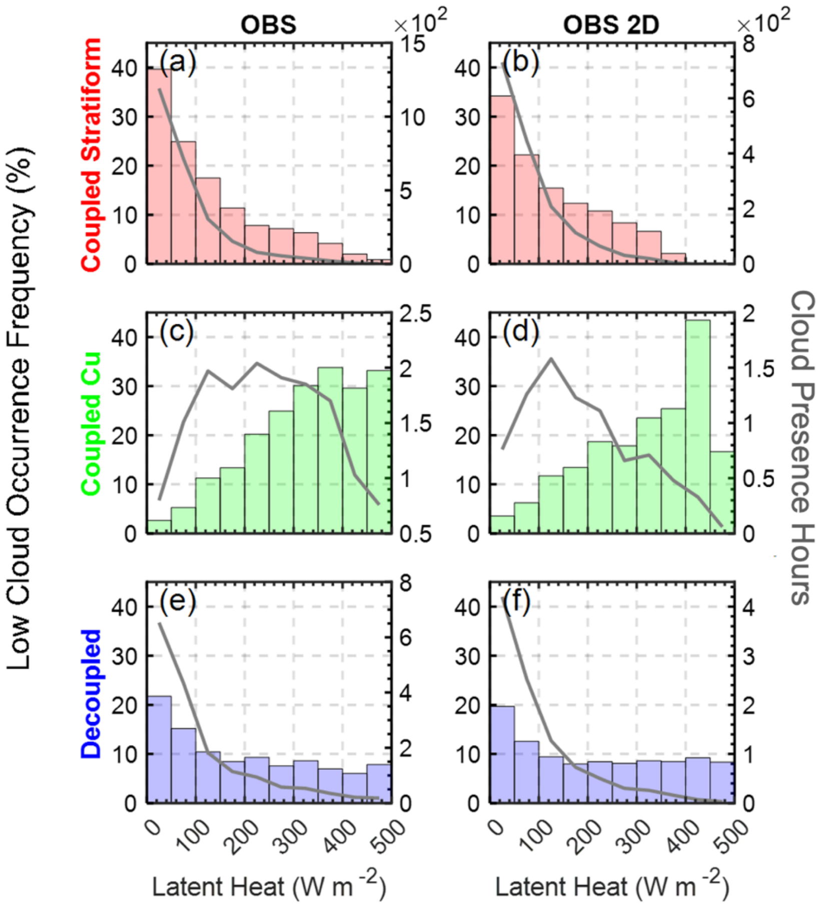

Figure S6. Similar to Figure S5, but depicting the relationships between low cloud occurrence frequency and surface latent heat fluxes.

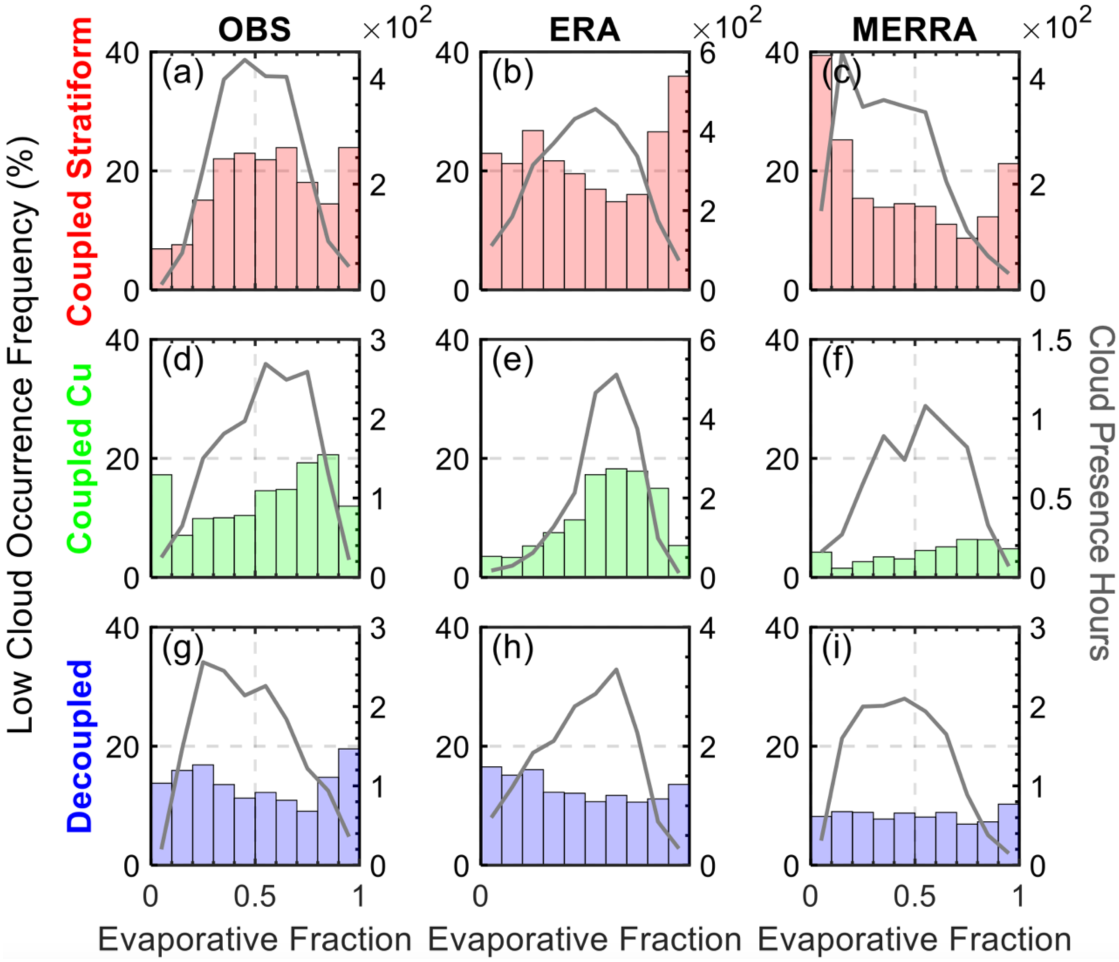

Figure S7. Similar to Figure S5, but depicting the relationships between low cloud occurrence frequency and evaporative fraction. Evaporative fraction is calculated as $\frac{Latent\ Heat}{Latent\ Heat+Sensible\ Heat}$.

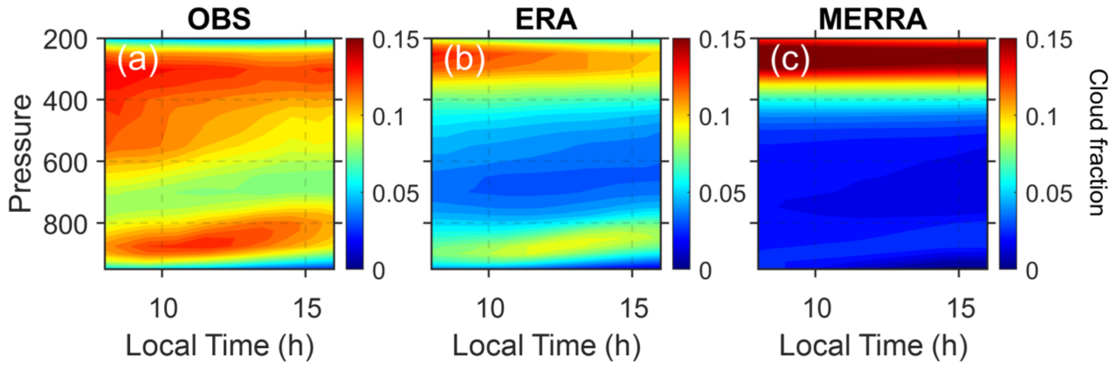

Figure S8. Diurnal Variation of Cloud Fraction in Observations and Reanalysis Data. Contour plots represent the diurnal cycle of cloud fraction as a function of pressure (in hPa) for observational (OBS, a) and two reanalysis datasets (ERA and MERRA, b-c).

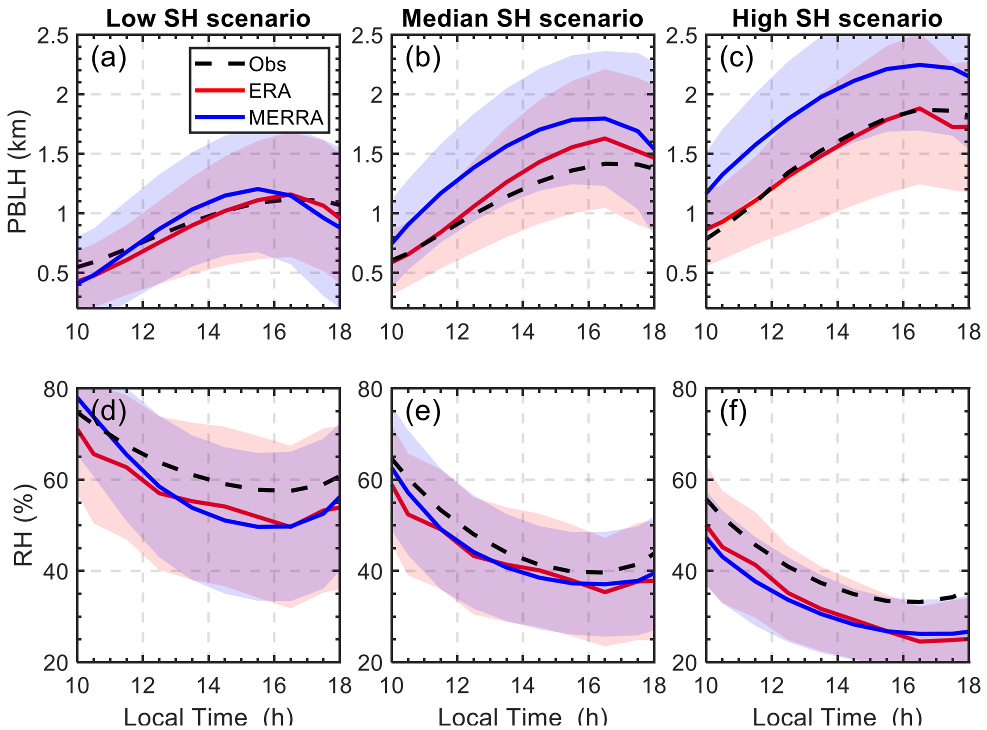

Figure S9. Diurnal variations in PBLH and RH across different sensible heat (SH) scenarios. The graphs illustrate the progression of PBLH and RH throughout the day, segmented into three sensible heat categories: low (0-200) (a, d), median (200-400) (b, e), and high (>400 W m^{-2}) (c, f). Solid lines represent the mean values from observations (Obs), ERA-5 reanalysis (ERA), and MERRA-2 reanalysis (MERRA). Shaded areas indicate one standard deviation from the mean, providing a visual representation of variability within each dataset.

References

Clothiaux, E. E., Ackerman, T. P., Mace, G. G., Moran, K. P., Marchand, R. T., Miller, M. A., & Martner, B. E. (2000). Objective determination of cloud heights and radar reflectivities using a combination of active remote sensors at the ARM CART sites. Journal of Applied Meteorology, 39(5), 645-665.

Gelaro, R., McCarty, W., Suárez, M.J., Todling, R., Molod, A., Takacs, L., Randles, C.A., Darmenov, A., Bosilovich, M.G., Reichle, R. and Wargan, K., 2017. The modern-era retrospective analysis for research and applications, version 2 (MERRA-2). Journal of climate, 30(14), pp.5419-5454.

Hersbach, H., Bell, B., Berrisford, P., Hirahara, S., Horányi, A., Muñoz-Sabater, J., Nicolas, J., Peubey, C., Radu, R., Schepers, D. and Simmons, A., 2020. The ERA5 global reanalysis. Quarterly Journal of the Royal Meteorological Society, 146(730), pp.1999-2049.

Holdridge, D., Ritsche, M., Prell, J., and Coulter, R. (2011): Balloon-borne sounding system (SONDE) handbook, https://www.arm.gov/capabilities/instruments/sonde.

Liu, S., & Liang, X. Z. (2010). Observed diurnal cycle climatology of planetary boundary layer height. Journal of Climate, 23(21), 5790-5809.

Schaaf, C.B., Gao, F., Strahler, A.H., Lucht, W., Li, X., Tsang, T., Strugnell, N.C., Zhang, X., Jin, Y., Muller, J.P. and Lewis, P., 2002. First operational BRDF, albedo nadir reflectance products from MODIS. Remote sensing of Environment, 83(1-2), pp.135-148.

Xie, S., McCoy, R.B., Klein, S.A., Cederwall, R.T., Wiscombe, W.J., Clothiaux, E.E., Gaustad, K.L., Golaz, J.C., Hall, S.D., Jensen, M.P. and Johnson, K.L., 2010. Clouds and more: ARM climate modeling best estimate data: A new data product for climate studies. Bulletin of the American Meteorological Society, 91(LLNL-JRNL-412676).